Signal Processing 141 (2017) 187–198

Contents lists available at ScienceDirect

Signal Processing

journal homepage: www.elsevier.com/locate/sigpro

Multistatic passive detection with parametric modeling of the IO waveform☆

Xin Zhang[a], Hongbin Li[a,*], Braham Himed[b]

[a] Department of Electrical and Computer Engineering, Stevens Institute of Technology, Hoboken, NJ 07030 USA
[b] AFRL/RYMD, Dayton, OH 45433 USA

ARTICLE INFO

Article history:
Received 15 December 2016
Revised 31 May 2017
Accepted 5 June 2017

Keywords:
Passive radar
Parametric multistatic detection
Auto-regressive process
Waveform correlation

ABSTRACT

This paper examines the target detection problem for a passive multistatic radar employing illuminators of opportunity (IOs), where the receivers are contaminated by non-negligible noise and direct-path interference (DPI). A parametric approach is proposed by modeling the unknown signal transmitted from the IO as an auto-regressive (AR) process whose temporal correlation is jointly estimated and exploited for passive detection. The proposed solution is developed based on the generalized likelihood ratio test principle, which involves non-linear estimation that is solved by using the expectation-maximization (EM) algorithm. We also discuss the initialization of the EM algorithm and the joint adaptive model order estimation for the AR process without using any training signal. In addition, we extend several conventional passive detectors, which were introduced by assuming no DPI is present, to provide them with an ability to handle the DPI problem. A clairvoyant matched filtering (MF) detector is derived as well assuming the knowledge of the IO waveform. Extensive simulation results are presented, using simulated waveforms whose temporal correlation can be easily controlled, as well as practical IO waveforms transmitted by frequency modulation (FM) radio. The results show that the proposed EM-based passive detector outperforms conventional passive detectors due to the exploitation of the waveform correlation.

1. Introduction

By exploiting non-cooperative illuminators of opportunity (IOs), such as radio, television, and cellular signals, passive radar can detect and track targets of interest without requiring a dedicated transmitter [1–5]. Passive radar has several advantages compared with an active system, including its covertness, because of the lack of a transmitter. It is easier to deploy a passive radar without incurring additional spectrum usage. Furthermore, a passive radar can readily employ a multistatic configuration by accessing multiple IOs at different locations, which leads to spatial diversity and improved sensing capabilities [6,7].

Passive sensing is more challenging than its active counterpart. A primary reason is that the IO waveform is unknown to the receiver. There are two general approaches to deal with the unknown IO waveform. The first is to treat the IO waveform as a deterministic process. One popular solution within this category is the cross-correlation (CC) method [1,2,5,8], which employs a reference channel (RC) at the receiver to collect the direct-path (transmitter-to-receiver) signal and, in addition, a separate surveillance channel (SC) to collect the target echo. Then, a CC operation is conducted between the RC and SC, which resembles the matched filtering (MF) approach used in active radar. Specifically, the reference signal obtained by the RC plays the role of the transmitted signal in the MF. It should be noted that, while the MF is optimum as it maximizes the receiver output signal-to-noise ratio (SNR), the CC is sub-optimal due to the presence of noise in the RC. In fact, it has been shown in [9] that the CC is highly sensitive to the presence of such noise. Recently, new improved passive detectors were introduced that take into account the effect of noisy reference [10,11]. In particular, [10] considered a multi-input multi-output (MIMO) setup, assuming knowledge of the noise power, while [11] also examined the case when the noise power is unknown. Within the deterministic category, another group of solutions employ multi-channel observations (e.g., via multiple spatially distributed sensors) of the target echo [12–15]. Because of the inter-channel correlation, a separate RC is no longer needed.

The second approach to deal with the unknown IO waveform is to model it as a stochastic process. The simplest solution within

☆ This work was supported in part by a subcontract with Matrix Research, Inc., for research sponsored by the Air Force Research Laboratory and also by the National Science Foundation under grant ECCS-1609393.

* Corresponding author.
E-mail addresses: xzhang23@stevens.edu (X. Zhang), Hongbin.Li@stevens.edu (H. Li), braham.himed@us.af.mil (B. Himed).

http://dx.doi.org/10.1016/j.sigpro.2017.06.003
0165-1684/

this category is to treat the samples of the waveform as independent and identically distributed (i.i.d.) Gaussian variables, i.e., the waveform correlation is neglected. Two stochastic passive detectors were derived based on this idea in [11], under the assumption that the noise power is either known or unknown. In [16,17], two-channel passive detection problems of known-rank signals were considered, where the RC and SC were both equipped with multiple antennas and the IO waveforms were treated as temporally white complex Gaussian signals. Due to coding, modulation, pulse shaping, propagation effects, etc., the IO waveform is in general correlated and such correlation can be exploited to improve passive sensing performance. Along this line, [18] considered the problem of estimating the delay and Doppler frequency of a target signal in passive radar by modeling the IO waveform as a correlated Gaussian process with known correlation. In practice, the correlation is unknown and has to be estimated. In addition, the correlation may change over time. Therefore, it would be of interest to develop techniques that can adaptively estimate the correlation and use it for passive detection and estimation.

Another challenge in passive sensing is the need to deal with the direct-path interference (DPI), which is the direct transmission from the IO source to the passive receiver. The DPI is generally significantly stronger (by many tens to even over a hundred dB) compared to the target echo [19,20]. The effect of the DPI on the CC detector was analyzed in [9], which showed that a modest level of DPI can significantly degrade the detection performance of the CC. As such, a passive radar has to employ some interference cancellation technique, such as an adaptive antenna with a null formed in the direction of the IO, and/or a temporal filter that employs the reference signal in the RC to cancel the DPI [21–24]. Despite such cancellation, some residual DPI may still exist due to, e.g., limited array size and null depth [25]. As a result, the DPI may still be at a non-negligible power level compared with the target echo.

In this paper, we examine the target detection problem for a passive multistatic radar system, where the receivers are contaminated by non-negligible noise and DPI. We propose a parametric approach that models the unknown IO signal as an autoregressive (AR) process, whose temporal correlation is estimated and exploited online for passive detection. We develop a solution using the generalized likelihood ratio test (GLRT) framework. Since the maximum likelihood estimates (MLEs) of the unknown parameters required by the GLRT cannot be obtained in closed form, we resort to an expectation-maximization (EM) procedure [26] to find these estimates. The initialization of the EM algorithm is discussed as well. We also examine adaptive joint model order selection for the AR process, parameter estimation, and detection. Additionally, we extend several well-known passive detectors, which originally assume the absence of DPI, to provide them with the ability to handle the DPI problem. For benchmarking, a clairvoyant MF detector is derived with the knowledge of the IO waveform. Extensive simulation results are presented to illustrate the effectiveness of the proposed detector relative to several representative solutions. These results are obtained using simulated waveforms whose temporal correlation can be easily controlled to examine the impact of the waveform correlation on passive detection, as well as practical IO waveforms transmitted by a frequency modulation (FM) radio.

The remainder of the paper is organized as follows. In Section 2, we present the system model and formulate the problem of interest. In Section 3, the proposed GLRT like detector[1] is derived. Extensions of conventional detectors and the benchmark detector are presented in Section 4. Numerical results and discussions are included in Section 5, followed by conclusions in Section 6.

[1] Strictly speaking, the proposed detector is not an exact GLRT because of the use of the EM estimates instead of the exact MLEs. With some notational abuse, the proposed detector will be referred to as the GLRT for simplicity.

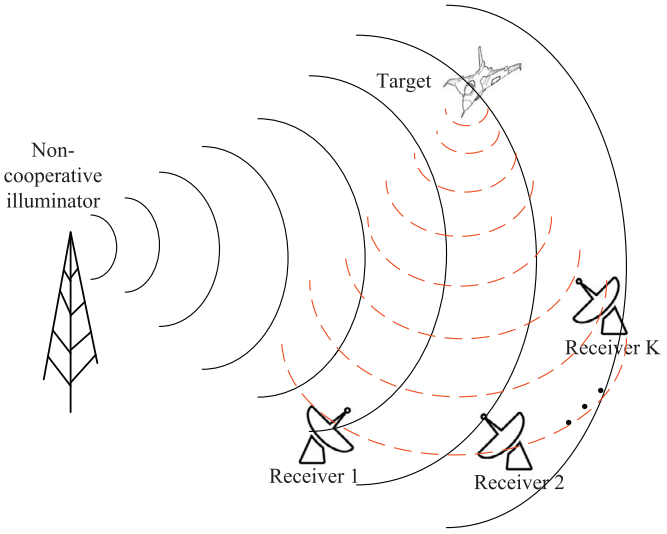

Fig. 1. Configuration of a multistatic passive radar system (dashed red line represents the reflection from the target). (For interpretation of the references to colour in this figure legend, the reader is referred to the web version of this article.)

Notation: Vectors (matrices) are denoted by boldface lower (upper) case letters, and all vectors are column vectors. Superscripts $(\cdot)^*$, $(\cdot)^T$, and $(\cdot)^H$ denote complex conjugate, transpose, and complex conjugate transpose, respectively. $\Re\{\cdot\}$ represents the real part of a complex quantity, $E\{\cdot\}$ denotes statistical expectation, and $\jmath$ stands for the imaginary unit. $\mathbf{0}_{p\times q}$ denotes a $p\times q$ matrix with all zero entries, $\mathbf{I}_N$ denotes an identity matrix of size N, $[\,\cdot\,]_{m,n}$ denotes the (m,n)th entry of a matrix, and $[\,\cdot\,]_m$ denotes the mth element of a vector. $\odot$ and $\otimes$ stand for the Hadamard and the Kronecker products, respectively. The notation $\mathcal{CN}$ denotes a circularly symmetric, complex Gaussian distribution. $\det\{\cdot\}$ represents the determinant of a matrix, $\|\cdot\|$ is the Frobenius norm, and $\mathrm{tr}\{\cdot\}$ denotes the trace of a matrix.

2. Problem formulation

Consider a multistatic passive radar system, as shown in Fig. 1, which contains one non-cooperative illuminator of opportunity (IO) and K distributed receivers. The signal collected by the kth receiver (channel) in the presence of a target, denoted by $y'_k(t)$, can be expressed as

$$y'_k(t) = \beta_k x(t-d_k) + \alpha'_k x(t-t_k)e^{\jmath 2\pi f_k t} + n'_k(t), \quad k=1,2,\ldots,K, \tag{1}$$

where $x(t)$ is the unknown signal (baseband equivalent) transmitted by the IO, d_k is the propagation delay from the IO to the kth receiver, i.e., the propagation delay of the DPI, t_k is the propagation delay of the target, due to the transmission from the IO to the target and then from the target to the kth receiver, f_k is the target's Doppler frequency seen at the kth receiver, β_k is the scaling coefficient which includes the antenna attenuation and the channel propagation effects from the IO to the kth receiver, α'_k is the scaling coefficient accounting for the target reflectivity, the antenna gain, and the channel propagation effects, and $n'_k(t)$ is the additive zero-mean white Gaussian noise at the kth channel.

To simplify the system model, we observe that the direct-path delay d_k is generally known a priori and can be compensated for, since the location of the IO is usually known to each receiver. Let $y_k(t) = y'_k(t+d_k)$ denote the kth delay-compensated signal, and the delay-compensated noise $n_k(t)$ is similarly defined. This leads to

$$y_k(t) = \beta_k x(t) + \alpha_k x(t-\tau_k)e^{\jmath 2\pi f_k t} + n_k(t), \tag{2}$$

where τ_k is the kth bistatic delay given by $\tau_k = t_k - d_k$ and $\alpha_k = \alpha_k' e^{j2\pi f_k d_k}$.

We assume that $x(t)$ has a duration of T seconds, e.g., due to the framed transmissions employed by the IO, in which case T represents the frame duration. The observation interval T_o is selected such that $T_o \geq T + \tau_{\max}$, where $\tau_{\max}$ denotes the maximum bistatic delay that can be tolerated by the system. We sample each channel using a sampling frequency $f_s \geq 2(B + f_{\max})$, where B denotes the bandwidth of the signal $x(t)$ and $f_{\max}$ is the maximum Doppler frequency of the target that is designed detectable by the system. Suppose M samples are collected for each channel over the observation window T_o, i.e., $T_o = MT_s$, where $T_s = 1/f_s$ denotes the sampling interval. Let $\mathbf{y}_k$, $\mathbf{x}$, and $\mathbf{n}_k$ be $M \times 1$ vectors formed by M adjacent samples of $y_k(t)$, $x(t)$, and $n_k(t)$, respectively. In addition, the M-point discrete Fourier transform (DFT) matrix $\mathbf{T}$ has entries $[\mathbf{T}]_{p,q} = e^{-j2\pi(p-1)\Delta f(q-1)T_s}/\sqrt{M}$, $p, q = 1, 2, \ldots, M$, with the frequency domain sample spacing $\Delta f = \frac{f_s}{M} = \frac{1}{T_s M}$, and $\mathbf{W}(x)$ is a diagonal matrix with diagonal entries $[\mathbf{W}(x)]_{p,p} = e^{j2\pi(p-1)x}$, $p = 1, 2, \ldots, M$. The discretized model can be written as [13,27]

$$\mathbf{y}_k = \beta_k \mathbf{x} + \alpha_k \mathcal{D}(\tau_k, f_k)\mathbf{x} + \mathbf{n}_k, \quad k = 1, 2, \ldots, K, \tag{3}$$

where the channel noise $\mathbf{n}_k$ is a zero-mean white Gaussian noise with variance η_k and

$$\mathcal{D}(\tau_k, f_k) = \mathbf{W}(f_k T_s)\mathbf{T}^H \mathbf{W}(-\tau_k \Delta f)\mathbf{T}. \tag{4}$$

In this paper, the signal waveform $\mathbf{x}$ is modeled as a correlated stochastic process with unit average power per sample. The temporal correlation of the waveform is usually unknown. In particular, we use an auto-regressive (AR) model to fit the stochastic IO waveform where the temporal correlation is parameterized by the AR coefficients and the zero-mean driving noise variance. The AR model has been widely used to model various correlated random processes in speech processing [28], wireless channel estimation [29], radar clutter modeling and cancellation [30,31], etc. A Pth order AR process is described by

$$x(n) = -\sum_{p=1}^{P} a(p)x(n-p) + w(n), \quad n = 1, 2, \ldots, N, \tag{5}$$

where $N = \lfloor \frac{T}{T_s} + 1 \rfloor \leq M$ is the number of the non-zero IO signal samples out of M observations, and $w(n) \sim \mathcal{CN}(0, \sigma^2)$ is the zero-mean driving noise. Consequently, $\mathbf{x}$ is a zero-mean Gaussian vector with covariance matrix $\mathbf{C}_x(\mathbf{a}, \sigma^2)$ which is parameterized by $\mathbf{a} \triangleq [a(1), a(2), \ldots, a(P)]^T$ and σ^2. The covariance matrix is Hermitian, Toeplitz, and fully determined by the auto-correlation function (ACF) sequence $\{r_x(n)\}$ as

$$\begin{bmatrix} r_x(0) & r_x^*(1) & \cdots & r_x^*(M-1) \\ r_x(1) & r_x(0) & \cdots & r_x^*(M-2) \\ \vdots & \vdots & \ddots & \vdots \\ r_x(M-1) & r_x(M-2) & \cdots & r_x(0) \end{bmatrix}.$$

The ACF sequence is related to the AR parameters $\mathbf{a}$ and σ^2 by the *Yule-Walker* equation [32]

$$r_x(n) = \begin{cases} -\sum_{p=1}^{P} a(p) r_x(n-p) & \text{for } n \geq 1 \\ -\sum_{p=1}^{P} a(p) r_x(-p) + \sigma^2 & \text{for } n = 0 \end{cases}, \tag{6}$$

where $r_x(n) = r_x^*(-n)$ for $n < 0$. Note that $r_x(0) = 1$ due to the unit power assumption for the IO signal. The problem of interest is to determine if a target is present in the cell of interest (test cell) using the observations $\{\mathbf{y}_k\}$. For each cell under test, the detection problem can be described by the following composite binary hypothesis test [10,11,13,14,33]:

$$\mathcal{H}_1 : \mathbf{y}_k = \beta_k \mathbf{x} + \alpha_k \mathcal{D}(\tau_k, f_k)\mathbf{x} + \mathbf{n}_k$$
$$\mathcal{H}_0 : \mathbf{y}_k = \beta_k \mathbf{x} + \mathbf{n}_k, \quad k = 1, 2, \ldots, K, \tag{7}$$

where the unknown parameters are the AR coefficients $\mathbf{a}$, σ^2, $\boldsymbol{\beta} = [\beta_1, \beta_2, \ldots, \beta_K]^T$, $\boldsymbol{\alpha} = [\alpha_1, \alpha_2, \ldots, \alpha_K]^T$, and $\boldsymbol{\eta} = [\eta_1, \eta_2, \ldots, \eta_K]^T$. In radar detection problem, it is customary to divide the uncertainty region of the target delay and Doppler frequency into small cells and each cell is tested for the presence of a target [34]. Therefore, for each cell under test, $\mathcal{D}(\tau_k, f_k)$ is known because the delay and Doppler associated with that cell is known and will be denoted as $\mathcal{D}_k$.

3. Proposed detector

In this section, we develop a GLRT like detector for the passive multistatic detection problem (7). The GLRT principle requires the maximum likelihood estimates (MLEs) of the unknown parameters under both hypotheses. Let the observations from K receivers be vectorized as $\mathbf{y} = [\mathbf{y}_1^T, \mathbf{y}_2^T, \ldots, \mathbf{y}_K^T]^T$. We can rewrite the detection problem (7) as

$$\mathcal{H}_1 : \mathbf{y} \sim \mathcal{CN}(\mathbf{0}_{MK\times 1}, \mathbf{C}_y(\boldsymbol{\alpha}, \boldsymbol{\beta}, \boldsymbol{\eta}, \mathbf{a}, \sigma^2))$$
$$\mathcal{H}_0 : \mathbf{y} \sim \mathcal{CN}(\mathbf{0}_{MK\times 1}, \mathbf{C}_y(\boldsymbol{\alpha} = \mathbf{0}, \boldsymbol{\beta}, \boldsymbol{\eta}, \mathbf{a}, \sigma^2)), \tag{8}$$

where the covariance matrix is given by

$$\begin{aligned} &\mathbf{C}_y(\boldsymbol{\alpha}, \boldsymbol{\beta}, \boldsymbol{\eta}, \mathbf{a}, \sigma^2) \\ &= (\boldsymbol{\beta}\boldsymbol{\beta}^H) \otimes \mathbf{C}_x(\mathbf{a}, \sigma^2) + [(\boldsymbol{\beta}\boldsymbol{\alpha}^H) \otimes \mathbf{C}_x(\mathbf{a}, \sigma^2)]\mathbf{D}^H \\ &\quad + \mathbf{D}[(\boldsymbol{\alpha}\boldsymbol{\beta}^H) \otimes \mathbf{C}_x(\mathbf{a}, \sigma^2)] + \mathbf{C}_n(\boldsymbol{\eta}) \\ &\quad + \mathbf{D}[(\boldsymbol{\alpha}\boldsymbol{\alpha}^H) \otimes \mathbf{C}_x(\mathbf{a}, \sigma^2)]\mathbf{D}^H, \end{aligned} \tag{9}$$

with block diagonal matrices $\mathbf{C}_n(\boldsymbol{\eta}) = \text{diag}\{\boldsymbol{\eta}\} \otimes \mathbf{I}_M$ and $\mathbf{D} = \text{diag}\{\mathcal{D}_1, \mathcal{D}_2 \ldots, \mathcal{D}_K\}$. Then, the GLRT is given by

$$\frac{\max_{\{\boldsymbol{\alpha}, \boldsymbol{\beta}, \boldsymbol{\eta}, \mathbf{a}, \sigma^2\}} p_1(\mathbf{y}|\boldsymbol{\alpha}, \boldsymbol{\beta}, \boldsymbol{\eta}, \mathbf{a}, \sigma^2)}{\max_{\{\boldsymbol{\beta}, \boldsymbol{\eta}, \mathbf{a}, \sigma^2\}} p_0(\mathbf{y}|\boldsymbol{\beta}, \boldsymbol{\eta}, \mathbf{a}, \sigma^2)} \underset{\mathcal{H}_0}{\overset{\mathcal{H}_1}{\gtrless}} \gamma, \tag{10}$$

where $p_1(\mathbf{y}|\boldsymbol{\alpha}, \boldsymbol{\beta}, \boldsymbol{\eta}, \mathbf{a}, \sigma^2)$ and $p_0(\mathbf{y}|\boldsymbol{\beta}, \boldsymbol{\eta}, \mathbf{a}, \sigma^2)$ denote the likelihood functions under $\mathcal{H}_1$ and $\mathcal{H}_0$, respectively. The two maximum likelihood estimation problems in (10) do not have closed-form solutions. A brute force search over the multi-dimensional parameter space is computationally intensive. Therefore, we resort to the EM algorithm to solve the maximum likelihood estimation problems, and the estimates are used in the GLRT detector.

To apply the EM algorithm under each hypothesis, the first step is to specify the "complete" data $\mathbf{z}$, which includes the observed data $\mathbf{y}$ (regarded as the "incomplete" data) [26]. In our case, the "complete" data is specified as

$$\mathbf{z} = [\mathbf{x}^T, \ \mathbf{y}^T]^T. \tag{11}$$

After determining the "complete" data, the EM algorithm starts with an initial guess of the unknown parameters, $\hat{\boldsymbol{\theta}}^{(0)}$ ($\boldsymbol{\theta} = \{\boldsymbol{\alpha}, \boldsymbol{\beta}, \boldsymbol{\eta}, \mathbf{a}, \sigma^2\}$ under $\mathcal{H}_1$; $\boldsymbol{\theta} = \{\boldsymbol{\beta}, \boldsymbol{\eta}, \mathbf{a}, \sigma^2\}$ under $\mathcal{H}_0$). Given the latest update for the parameter estimation after l iterations, $\hat{\boldsymbol{\theta}}^{(l)}$, the $(l+1)$th iteration consists of an expectation step (E-step) followed by a maximization step (M-step):

E-step:

$$Q\left(\boldsymbol{\theta}; \hat{\boldsymbol{\theta}}^{(l)}\right) = E_{\mathbf{x}|\mathbf{y}, \hat{\boldsymbol{\theta}}^{(l)}}\left\{\log p(\mathbf{z}|\boldsymbol{\theta})\right\}. \tag{12}$$

M-step:

$$\hat{\boldsymbol{\theta}}^{(l+1)} = \arg\max_{\boldsymbol{\theta}} Q\left(\boldsymbol{\theta}; \hat{\boldsymbol{\theta}}^{(l)}\right). \tag{13}$$

The E-step is intended to find the expectation of the log-likelihood function (LLF) of the "complete" data $\mathbf{z}$, which is taken

with respect to the signal waveform $\mathbf{x}$ and conditioned on observations $\mathbf{y}$ given $\hat{\boldsymbol{\theta}}^{(l)}$. The M-step is intended to maximize the expectation with respect to the unknown parameters. This iteration cycle is repeated until the algorithm converges, e.g., when the following inequality holds for some small tolerance ϵ:

$$\left\|\hat{\boldsymbol{\theta}}^{(l+1)}-\hat{\boldsymbol{\theta}}^{(l)}\right\|<\epsilon. \tag{14}$$

In the following, we discuss the details of using the EM algorithm to find estimates of the unknown parameters under the two hypotheses.

3.1. Parameter estimation under $\mathcal{H}_1$

Here, we derive the MLEs of the unknown parameters under $\mathcal{H}_1$ by assuming knowledge of the AR model order P. In Section 3.5, we will discuss how to determine the AR model order through standard model order selection criteria.

It is shown in Appendix A that, for the $(l+1)$th iteration, the M-step (13) under $\mathcal{H}_1$ is equivalent to

$$\hat{\boldsymbol{\theta}}^{(l+1)}=\arg\min_{\boldsymbol{\theta}} Q_1\left(\boldsymbol{\theta};\hat{\boldsymbol{\theta}}^{(l)}\right), \tag{15}$$

where

$$Q_1\left(\boldsymbol{\theta};\hat{\boldsymbol{\theta}}^{(l)}\right)=(M-P)\ln\sigma^2+\frac{\hat{\Delta}_1^{(l)}(\mathbf{a})}{\sigma^2}+\sum_{k=1}^{K}\left(M\ln\eta_k+\frac{\hat{\Delta}_2^{(l)}(\alpha_k,\beta_k)}{\eta_k}\right), \tag{16}$$

with

$$\hat{\Delta}_1^{(l)}(\mathbf{a})=c_5^{(l)}+(\mathbf{c}_6^{(l)})^H\mathbf{a}+\mathbf{a}^H\mathbf{c}_6^{(l)}+\mathbf{a}^H\mathbf{C}_7^{(l)}\mathbf{a}, \tag{17}$$

$$\hat{\Delta}_2^{(l)}(\alpha_k,\beta_k)=\|\mathbf{y}_k\|^2+\left(|\beta_k|^2+|\alpha_k|^2\right)c_1^{(l)}+2\Re\left\{\alpha_k\beta_k^*c_{2,k}^{(l)}-\beta_k c_{3,k}^{(l)}-\alpha_k c_{4,k}^{(l)}\right\}. \tag{18}$$

From (16), it can be seen that the unknown parameters are well separated into $K+1$ subsets, i.e., $\{\mathbf{a},\ \sigma^2\}$ and $\{\alpha_k,\ \beta_k,\ \eta_k\}$ for $k=1,2,\ldots,K$. The cost functions (17) and (18) are quadratic with respect to $\{\mathbf{a}\}$ and $\{\alpha_k,\ \beta_k\}$, respectively, and thus admit closed-form solutions. Through standard manipulations, we have

$$\hat{\mathbf{a}}^{(l+1)}=-\left(\mathbf{C}_7^{(l)}\right)^{-1}\mathbf{c}_6^{(l)}, \tag{19}$$

$$\hat{\sigma^2}^{(l+1)}=\frac{1}{M-P}\left(c_5^{(l)}-\left(\mathbf{c}_6^{(l)}\right)^H\left(\mathbf{C}_7^{(l)}\right)^{-1}\mathbf{c}_6^{(l)}\right) \tag{20}$$

$$\hat{\alpha}_k^{(l+1)}=\frac{\left(c_1^{(l)}c_{4,k}^{(l)}-c_{2,k}^{(l)}c_{3,k}^{(l)}\right)^*}{\left(c_1^{(l)}\right)^2-\left|c_{2,k}^{(l)}\right|^2}, \tag{21}$$

$$\hat{\beta}_k^{(l+1)}=\frac{c_1^{(l)}\left(c_{3,k}^{(l)}\right)^*-c_{2,k}^{(l)}\left(c_{4,k}^{(l)}\right)^*}{\left(c_1^{(l)}\right)^2-\left|c_{2,k}^{(l)}\right|^2}, \tag{22}$$

$$\hat{\eta}_k^{(l+1)}=\frac{1}{M}\hat{\Delta}_2^{(l)}\left(\hat{\alpha}_k^{(l+1)},\hat{\beta}_k^{(l+1)}\right). \tag{23}$$

3.2. Parameter estimation under $\mathcal{H}_0$

Under $\mathcal{H}_0$, the received data is free of target echoes, and the unknown parameters are $\boldsymbol{\theta}=\{\boldsymbol{\beta},\boldsymbol{\eta},\mathbf{a},\sigma^2\}$. The MLEs under this hypothesis can be obtained by repeating the steps under $\mathcal{H}_1$ with $\boldsymbol{\alpha}$ set to zero. As a result, we have

$$\hat{\beta}_k^{(l+1)}=\frac{\left(c_{3,k}^{(l)}\right)^*}{c_1^{(l)}}, \tag{24}$$

$$\hat{\eta}_k^{(l+1)}=\frac{1}{M}\hat{\Delta}_2^{(l)}\left(0,\hat{\beta}_k^{(l+1)}\right), \tag{25}$$

while $\hat{\mathbf{a}}^{(l+1)}$ and $\hat{\sigma^2}^{(l+1)}$ have the same expressions as in (19) and (20), respectively. It is worth mentioning that, when conducting the E-step calculations in this case, $\hat{\boldsymbol{\alpha}}^{(l)}$ should also be treated as zero.

3.3. Parameter initialization

In this section, we discuss an initialization method that can be used to start the EM algorithm. First, the EM algorithm requires an initialization of the waveform covariance matrix which depends on the AR coefficients $\mathbf{a}$ and the variance σ^2 of the driving noise. The covariance matrix is initialized as $\hat{\mathbf{C}}_x^{(0)}=\mathbf{I}_M$ under both hypotheses. In other words, the waveform correlation is ignored for the start-up of the EM algorithm. Next, we discuss the initialization of the related channel parameters, including the amplitudes and the channel noise variances. The initialization of these parameters is based on a principal eigenvector (PEV) method, which is detailed in Section 4.1. First, we use the PEV method to obtain an initial estimate of the waveform $\mathbf{x}$, and then coarse estimates of the amplitudes and channel noise variances are obtained through cross-correlation. Denote the waveform estimates under $\mathcal{H}_1$ and $\mathcal{H}_0$ as $\bar{\mathbf{x}}_1$ and $\bar{\mathbf{x}}_0$, respectively. We initialize the amplitudes and the channel noise variances under $\mathcal{H}_1$ as [18]

$$\hat{\alpha}_k^{(0)}=\frac{b_2b_{4,k}-b_{1,k}b_{3,k}^*}{b_2^2-|b_{3,k}|^2}, \tag{26}$$

$$\hat{\beta}_k^{(0)}=\frac{b_{1,k}b_2-b_{3,k}b_{4,k}}{b_2^2-|b_{3,k}|^2}, \tag{27}$$

where $b_{1,k}=\bar{\mathbf{x}}_1^H\mathbf{y}_k$, $b_2=\|\bar{\mathbf{x}}_1\|^2$, $b_{3,k}=\bar{\mathbf{x}}_1^H\mathcal{D}_k\bar{\mathbf{x}}_1$, and $b_{4,k}=\bar{\mathbf{x}}_1^H\mathcal{D}_k^H\mathbf{y}_k$, and

$$\hat{\eta}_k^{(0)}=\frac{1}{M}\left\|\mathbf{y}_k-\hat{\beta}_k^{(0)}\bar{\mathbf{x}}_1-\hat{\alpha}_k^{(0)}\mathcal{D}_k\bar{\mathbf{x}}_1\right\|^2. \tag{28}$$

Under $\mathcal{H}_0$, we have

$$\hat{\beta}_k^{(0)}=\frac{\bar{\mathbf{x}}_0^H\mathbf{y}_k}{\|\bar{\mathbf{x}}_0\|^2}, \tag{29}$$

and

$$\hat{\eta}_k^{(0)}=\frac{1}{M}\left\|\mathbf{y}_k-\hat{\beta}_k^{(0)}\bar{\mathbf{x}}_0\right\|^2. \tag{30}$$

3.4. Detection algorithm

From the derivations in Sections 3.1 and 3.2, we notice that the M-step of the EM-based estimation algorithm consists of two estimation processes. The first deals with estimating the coefficients related to the AR model, i.e., $\mathbf{a}$ and σ^2, and the second one is for amplitude and channel noise variance estimation. The former is obtained by least-squares (LS) via (19). Another popular method for AR coefficient estimation is the auto-correlation (AC) method [35], which tends to perform better for our problem. For easy reference, the AC method is briefly summarized in Appendix B.

Once the EM iteration converges, let $\hat{\boldsymbol{\theta}}_1=\{\hat{\boldsymbol{\alpha}}_1,\hat{\boldsymbol{\beta}}_1,\hat{\boldsymbol{\eta}}_1,\hat{\mathbf{a}}_1,\hat{\sigma}_1^2\}$ and $\hat{\boldsymbol{\theta}}_0=\{\hat{\boldsymbol{\beta}}_0,\hat{\boldsymbol{\eta}}_0,\hat{\mathbf{a}}_0,\hat{\sigma}_0^2\}$ be the final estimates of the unknown parameters under $\mathcal{H}_1$ and $\mathcal{H}_0$, respectively. The proposed detector can be written as

$$\begin{aligned}\mathcal{L}&=\log p_1(\mathbf{y}|\hat{\boldsymbol{\theta}}_1)-\log p_0(\mathbf{y}|\hat{\boldsymbol{\theta}}_0)\\&=\mathbf{y}^H\left[\mathbf{C}_y^{-1}(\mathbf{0},\hat{\boldsymbol{\theta}}_0)-\mathbf{C}_y^{-1}(\hat{\boldsymbol{\theta}}_1)\right]\mathbf{y}\end{aligned}$$

$$+\ln\frac{\det\left\{\mathbf{C}_y(\mathbf{0},\hat{\boldsymbol{\theta}}_0)\right\}}{\det\left\{\mathbf{C}_y(\hat{\boldsymbol{\theta}}_1)\right\}}\underset{\mathcal{H}_0}{\overset{\mathcal{H}_1}{\gtrless}}\xi, \tag{31}$$

where $\xi=\ln\gamma$. The proposed detector is summarized in Algorithm 1.

Algorithm 1 Proposed detector.

Input: K-channel observations $\mathbf{y}$, AR model order P, a specific delay-Doppler cell, initial guess of the parameters $\hat{\boldsymbol{\theta}}^{(0)}$, and convergence tolerance ϵ.
Output: $\mathcal{L}$ as computed by (31).
Estimation of $\boldsymbol{\theta}=\{\boldsymbol{\alpha},\boldsymbol{\beta},\boldsymbol{\eta},\mathbf{a},\sigma^2\}$ under $\mathcal{H}_1$:
for $l=0,1,2,\ldots$ **do**
1. Compute the results of E-step using (65)–(74) and (80)–(83).
2. Update the estimates of unknown parameters using (19)–(23) for $k=1,2,\ldots,K$.
3. Check the stopping condition (14).

end for
Estimation of $\boldsymbol{\theta}=\{\boldsymbol{\beta},\boldsymbol{\eta},\mathbf{a},\sigma^2\}$ under $\mathcal{H}_0$:
for $l=0,1,2,\ldots$ **do**
1. Compute the results of E-step using (65)–(70), (72), (74), and (80)–(83) with $\hat{\boldsymbol{\alpha}}^{(l)}=\mathbf{0}$.
2. Update the estimates of unknown parameters using (19), (20), (24), and (25) for $k=1,2,\ldots,K$.
3. Check the stopping condition (14).

end for
return

The computational complexity of the proposed algorithm is dominated by the update of the posterior mean (68) and posterior correlation matrix (69) in the E-step, which involves inverting an $MK\times MK$ matrix $\mathbf{C}_{yy}^{(l)}$ that is a structured matrix as defined in (9).

3.5. Model order selection

The above detector is developed under the assumption that the AR model order P is known a priori. In this section, we extend the proposed detector to provide joint adaptive model order estimation. In other words, the AR model order P is adaptively estimated from the observations. In practice, the model order can be determined by many model order selection techniques, such as the minimum description length (MDL) criterion or Akaike information criterion (AIC) [32]. Here, we consider the generalized Akaike information criterion (GAIC) due to its simplicity and accuracy [36]. Specifically, the GAIC combines the negative logarithmic likelihood function with a penalty term proportional to the model order. For our problem, the GAIC is shown as

$$\begin{aligned}\mathcal{H}_1:\hat{P}_1=&\arg\min_{P_1}[\mathbf{y}^H\mathbf{C}_y(\hat{\boldsymbol{\theta}}_1(P_1))\mathbf{y}\\&+\ln\det\left\{\mathbf{C}_y(\hat{\boldsymbol{\theta}}_1(P_1))\right\}\\&+\kappa(2P_1+5K+1)],\end{aligned} \tag{32}$$

$$\begin{aligned}\mathcal{H}_0:\hat{P}_0=&\arg\min_{P_0}[\mathbf{y}^H\mathbf{C}_y(\mathbf{0},\hat{\boldsymbol{\theta}}_0(P_0))\mathbf{y}\\&+\ln\det\left\{\mathbf{C}_y(\mathbf{0},\hat{\boldsymbol{\theta}}_0(P_0))\right\}\\&+\kappa(2P_0+3K+1)],\end{aligned} \tag{33}$$

where κ is a user parameter chosen as $\kappa=\frac{4M}{M-K-1}$ in our case. Particularly, the estimates $\hat{\boldsymbol{\theta}}_1(P_1)$ and $\hat{\boldsymbol{\theta}}_0(P_0)$ are obtained using the proposed EM-based algorithms, which are dependent on the tested AR model orders under $\mathcal{H}_1$ and $\mathcal{H}_0$, respectively.

4. Other passive detectors and extensions

There are several passive detectors, including the energy detector (ED) [37], the generalized canonical correlation (GCC) detector [33,38], the generalized coherence (GC) detector [39], and an eigenvalue-based detector [14], which were introduced by assuming the absence of DPI. As such, they cannot be directly applied to solve our detection problem as specified in Section 2. To provide these detectors with the ability to handle the DPI, the idea is to obtain an estimate of the DPI, followed by DPI cancellation. In the following, we first briefly discuss a DPI estimator based on the principal eigenvector (PEV) of the sample covariance matrix. Then, we introduce extensions of several existing passive detectors to deal with DPI. In addition, we also discuss a clairvoyant MF detector that assumes knowledge of the source waveform and propose an implementable MF detector modified from the clairvoyant MF.

4.1. PEV method for DPI estimation

The PEV method estimates the IO waveform as the normalized principal eigenvector of the sample covariance matrix of the observations [13,14]. Under $\mathcal{H}_0$, it is clear that an estimate of $\mathbf{x}$ is given by

$$\hat{\mathbf{x}}=\mathbf{v}_1\left(\mathbf{Y}\mathbf{Y}^H\right), \tag{34}$$

where $\mathbf{Y}=[\mathbf{y}_1,\mathbf{y}_2,\ldots,\mathbf{y}_K]$ and $\mathbf{v}_1(\cdot)$ represents the normalized principal eigenvector of a matrix. The above estimate also holds approximately under $\mathcal{H}_1$, since in practice the DPI is stronger than the target echo which can be neglected.

4.2. Modified existing passive detectors with DPI cancellation

Here, we extend several existing detectors by adding a DPI cancellation step based on the PEV method. Once we have the estimated IO waveform, the amplitude of the DPI in the kth channel can be estimated as

$$\hat{\beta}_k=\frac{\hat{\mathbf{x}}^H\mathbf{y}_k}{\hat{\mathbf{x}}^H\hat{\mathbf{x}}}. \tag{35}$$

Consequently, the signal after suppressing the DPI is

$$\tilde{\mathbf{y}}_k=\mathbf{y}_k-\hat{\beta}_k\hat{\mathbf{x}},\quad k=1,2,\ldots,K. \tag{36}$$

Then, $\{\tilde{\mathbf{y}}_k\}$ can be used to replace the original observation $\{\mathbf{y}_k\}$ in the existing detectors as modified versions. For instance, the modified energy detector (mED) and modified GCC (mGCC) detector are given by

$$\mathcal{L}_{\mathrm{mED}}=\sum_{k=1}^{K}\|\tilde{\mathbf{y}}_k\|^2\underset{\mathcal{H}_0}{\overset{\mathcal{H}_1}{\gtrless}}\gamma_{\mathrm{mED}}, \tag{37}$$

and

$$\mathcal{L}_{\mathrm{mGCC}}=\lambda_1\left(\tilde{\mathbf{Y}}^H\tilde{\mathbf{Y}}\right)\underset{\mathcal{H}_0}{\overset{\mathcal{H}_1}{\gtrless}}\gamma_{\mathrm{mGCC}}, \tag{38}$$

respectively, where $\tilde{\mathbf{Y}}=[\mathcal{D}_1^H\tilde{\mathbf{y}}_1,\mathcal{D}_2^H\tilde{\mathbf{y}}_2,\ldots,\mathcal{D}_K^H\tilde{\mathbf{y}}_K]$ and $\lambda_1(\cdot)$ is the principal eigenvalue of a K-dimensional matrix. The mED and the mGCC detector are used for comparisons in our simulations; other modified detectors can be formulated in a similar way.

4.3. A Clairvoyant matched filter in the presence of DPI

For comparison purposes, we also derive a clairvoyant MF detector under the GLRT framework. The detector is clairvoyant because it assumes the IO waveform is known and serves as an upper bound for all passive detectors considered in this paper. The likelihood function under $\mathcal{H}_1$ can be written as

$$p(\mathbf{y}|\boldsymbol{\alpha},\boldsymbol{\beta},\boldsymbol{\eta}) = \frac{1}{\pi^{MK}\prod_{k=1}^{K}\eta_k^M} \times \exp\left\{-\sum_{k=1}^{K}\frac{\|\mathbf{y}_k-\beta_k\mathbf{x}-\alpha_k\mathcal{D}_k\mathbf{x}\|^2}{\eta_k}\right\}. \tag{39}$$

The MLEs of the unknown parameters are

$$\left[\hat{\alpha}_{k,1},\hat{\beta}_{k,1}\right]^T = \left(\mathbf{H}_k^H\mathbf{H}_k\right)^{-1}\mathbf{H}_k^H\mathbf{y}_k, \tag{40}$$

where

$$\mathbf{H}_k = [\mathcal{D}_k\mathbf{x},\mathbf{x}], \tag{41}$$

and

$$\hat{\eta}_{k,1} = \frac{1}{M}\left\|\mathbf{P}_k^{\perp}\mathbf{y}_k\right\|^2, \tag{42}$$

where

$$\mathbf{P}_k^{\perp} = \mathbf{I}-\mathbf{H}_k\left(\mathbf{H}_k^H\mathbf{H}_k\right)^{-1}\mathbf{H}_k^H. \tag{43}$$

Under $\mathcal{H}_0$, the likelihood function is given by

$$p(\mathbf{y}|\boldsymbol{\beta},\boldsymbol{\eta}) = \frac{1}{\pi^{MK}\prod_{k=1}^{K}\eta_k^M} \times \exp\left\{-\sum_{k=1}^{K}\frac{\|\mathbf{y}_k-\beta_k\mathbf{x}\|^2}{\eta_k}\right\}. \tag{44}$$

It is easy to show that the MLEs are given by

$$\hat{\beta}_{k,0} = \left(\mathbf{x}^H\mathbf{x}\right)^{-1}\mathbf{x}^H\mathbf{y}_k, \tag{45}$$

and

$$\hat{\eta}_{k,0} = \frac{1}{M}\left\|\mathbf{P}_x^{\perp}\mathbf{y}_k\right\|^2, \tag{46}$$

where

$$\mathbf{P}_x^{\perp} = \mathbf{I}-\frac{1}{\|\mathbf{x}\|^2}\mathbf{x}\mathbf{x}^H. \tag{47}$$

Finally, the clairvoyant MF detector is the GLRT obtained by using the above MLEs in the likelihood functions (39) and (44):

$$\mathcal{L}_{\mathrm{MF}} = \prod_{k=1}^{K}\frac{\hat{\eta}_{k,0}}{\hat{\eta}_{k,1}} = \prod_{k=1}^{K}\frac{\left\|\mathbf{P}_x^{\perp}\mathbf{y}_k\right\|^2}{\left\|\mathbf{P}_k^{\perp}\mathbf{y}_k\right\|^2}. \tag{48}$$

5. Numerical simulations

In this section, numerical results are presented to illustrate the performance of the proposed techniques. In order to show the benefit of using an AR model to estimate and exploit the IO waveform correlation, we consider three implementations of the proposed GLRT. The first is referred to as the pGLRT, which stands for the *parametric GLRT* detector presented in Section 3 that utilizes an AR model for the IO waveform. The second, denoted as iGLRT, is an *ideal GLRT* that assumes knowledge of the covariance matrix $\mathbf{C}_x$ of the IO waveform. The third, denoted as sGLRT, is the *simple GLRT* when the covariance matrix $\mathbf{C}_x$ is replaced by an identity matrix, i.e., the correlation of the IO waveform is completely ignored for detection. Note that the latter two GLRT detectors do not involve an AR model as they assume a given waveform covariance

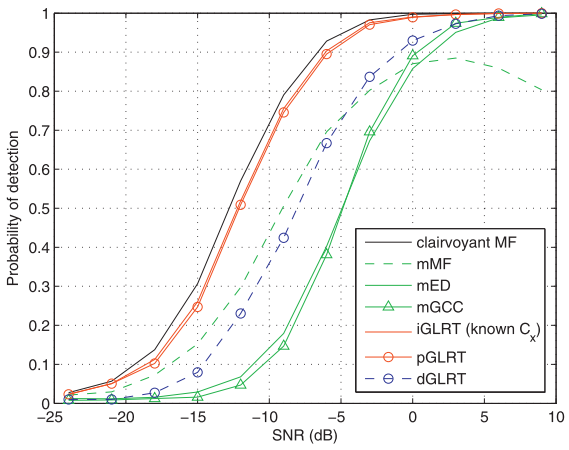

(a)

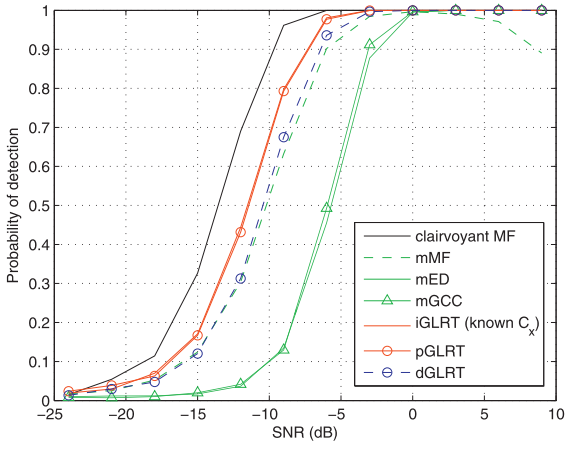

(b)

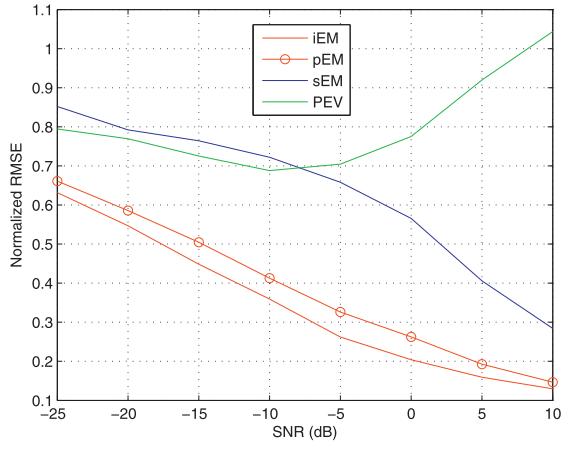

(c)

Fig. 2. Detection and estimation performance versus SNR with $M = 50$, $K = 3$, and DNR = 0 dB. Detection probability with (a) highly correlated waveform ($\rho = 0.9$) and (b) lowly correlated waveform ($\rho = 0.1$). (c) Normalized root mean-square error (RMSE) of waveform estimate with $\rho = 0.9$.

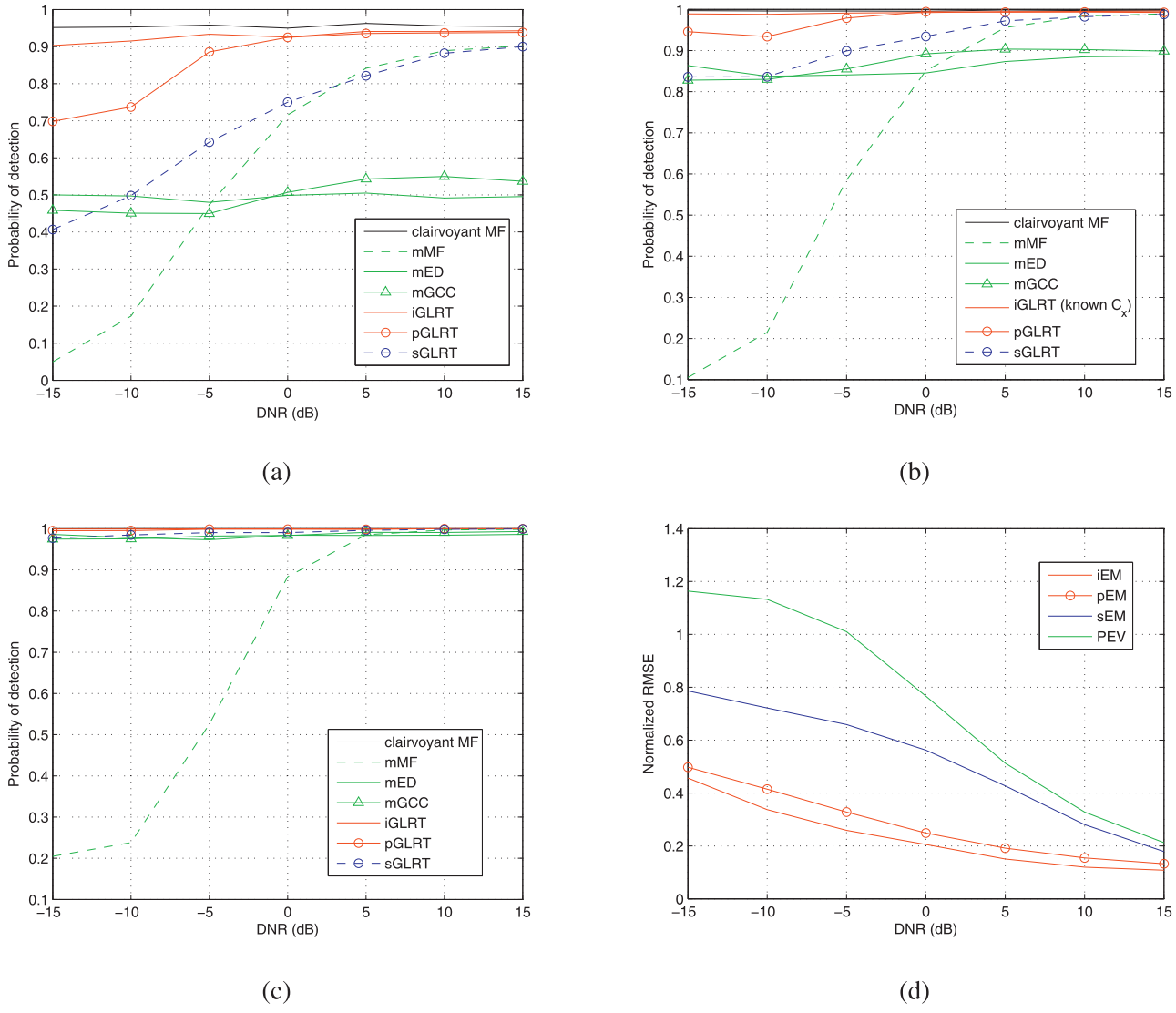

Fig. 3. Detection and estimation performance versus DNR with $M = 50$, $K = 3$, and $\rho = 0.9$. Detection probability with (a) SNR $= -5$ dB, (b) SNR $= 0$ dB, and (c) SNR $= 5$ dB. (d) Normalized RMSE of waveform estimate with SNR $= 0$ dB.

matrix. As we shall see, the pGLRT is able to approach the iGLRT, while the sGLRT may experience considerable degradation by not exploiting the waveform correlation for passive detection. In addition to the GLRT detectors, we also include the clairvoyant MF of Section 4.3 as a benchmark, the modified detectors mED and mGCC of Section 4.2, as well as a modified version of the clairvoyant MF, referred to as the mMF, for comparison purposes. The mMF replaces the true waveform with the PEV estimate (34) and thus represents a practical solution.

We consider two types of IO waveforms. The first is based on a stochastic model, where we can easily control/change the waveform temporal correlation, which allows us to examine the impact of correlation on passive detection. The second is an FM waveform as transmitted by an FM radio station, which corresponds to a more realistic passive sensing scenario.

5.1. Stochastic model based IO waveform

Here, the IO waveform is generated as a correlated stochastic process with a widely used Gaussian-shaped power spectral density (PSD) [40,41]. Specifically, the temporal correlation of the random process is given by

$$r(n) = P_x e^{-\frac{n^2}{2\sigma_r^2}}, \tag{49}$$

where P_x denotes the average power, n the correlation lag, and σ_r the standard deviation that specifies how rapidly the waveform fluctuates in time: a large value of σ_r implies that the waveform is highly correlated and vice versa. In our simulations, we choose $P_x = 1$ due to the unit power assumption. The IO waveform is statistically stationary with a Toeplitz covariance matrix $\mathbf{C}_x$ formed by samples of the temporal correlation: $r(0), r(1), \ldots, r(N-1)$. Note that the above random process is in general not an AR process. Therefore, by treating it as an AR process, there is a model mismatch in the proposed pGLRT detector. Nevertheless, as we shall see, the AR modeling is still able to effectively capture the temporal correlation of the random waveform, allowing us to exploit the correlation for passive detection. In the sequel, we will test different detectors under both *high correlation* and, respectively, *low correlation* scenarios, measured by the following correlation parameter

$$\rho = \frac{1}{N-1}\sum_{n=0}^{N-2}\left|\frac{r(n+1)}{r(n)}\right|. \tag{50}$$

The signal-to-noise ratio (SNR) is defined as

$$\mathrm{SNR} = \frac{1}{K}\sum_{k=1}^{K}\frac{N|\alpha_k|^2}{M\eta_k}, \tag{51}$$

and the DPI-to-noise ratio (DNR) is

$$\mathrm{DNR} = \frac{1}{K}\sum_{k=1}^{K}\frac{N|\beta_k|^2}{M\eta_k}. \tag{52}$$

The detection probability curves versus SNR are plotted in Fig. 2 where the observation length $M = 50$, channel number $K = 3$, and $\mathrm{DNR} = 0$ dB. In the simulations throughout this paper, the probability of detection is measured when the probability of false alarm is set to 10^{-2}. Two cases of different waveform correlations are considered in this scenario. From Fig. 2(a), where $\rho = 0.9$, we see that the performance of the proposed pGLRT detector is very close to that of the iGLRT detector, and the clairvoyant MF detector is slightly better. The sGLRT detector performs about 4 dB worse than the pGLRT detector. The mED and mGCC detectors have similar performances, which are nearly 7 dB worse than the pGLRT detector. The mMF performs quite well for low SNR. Its degradation at high SNR is caused by the PEV estimate of the waveform. As noted in Section 4.1, the PEV estimate is based on the assumption that the DPI is strong and the target is absent, which is seriously violated at high SNR. The poor PEV estimate at high SNR has a direct impact on the mMF, which relies on the estimated waveform for signal projection. The impact on the mED and mGCC, however, is less since both are energy based detectors.

Fig. 2(b) depicts the results of a low correlation case with $\rho = 0.1$. It is seen that the performance of the pGLRT detector can still approach that of the iGLRT detector; however, their performance gain over the sGLRT detector is not as significant as in the former case, since low correlation implies less information so that the improvement through exploiting the correlation is limited.

Fig. 2(c) shows waveform estimation performance of different estimators for the case of $\rho = 0.9$. It should be pointed out that waveform estimation has a multiplicative ambiguity due to the fact that both the amplitude parameters, α_k and β_k, and the waveform $\mathbf{x}$ in (7) are unknown. The ambiguity has to be accounted for before different waveform estimators can be compared with each other. Specifically, let $\hat{\mathbf{x}}$ be the waveform estimate obtained by any estimator. It is normalized as follows to remove the ambiguity: $\hat{\mathbf{x}}' = \frac{[\mathbf{x}]_1}{[\hat{\mathbf{x}}]_1}\hat{\mathbf{x}}$. Then, the normalized root mean-square error (RMSE), defined as $\sqrt{E\left\{\|\hat{\mathbf{x}}' - \mathbf{x}\|^2\right\}}/\|\mathbf{x}\|$, is used to measure the estimation accuracy. We consider the performance of the EM estimator with three implementations, namely with (1) a parametric AR model; (2) known covariance matrix $\mathbf{C}_x$; and (3) $\mathbf{C}_x = \mathbf{I}$, which corresponds to the EM estimator underlying the pGLRT, iGLRT, and sGLRT, respectively. These EM estimators are accordingly referred to as pEM, iEM, and sEM, respectively. In addition, the PEV estimator of Section 4.1 is also included for comparison. Fig. 2(c) shows the normalized RMSEs of the above estimators versus SNR under the $\mathcal{H}_1$ hypothesis, where the simulation parameters are the same as those in Fig. 2(a). We observe that the iEM method performs the best, and the pEM method is slightly worse. The sEM method performs much worse than the pEM method, since the former does not exploit the waveform correlation. The PEV performance gets worse as the SNR increases (high SNR region), due to the increased interference strength caused by the target signal.

Fig. 3 shows the numerical results versus DNR with $M = 50$, $K = 3$, and $\rho = 0.9$. Fig. 3(a)–(c) illustrate the detection performances when $\mathrm{SNR} = -5$ dB, 0 dB, and 5 dB, respectively. Interestingly, it is observed that the probabilities of detection for the proposed detectors improve at high DNR. The reason is that a stronger DPI, which contains information about the waveform, helps estimate the waveform. The evidence will be illustrated in Fig. 3(d). From these figures, we also see that the iGLRT detector performs the best, i.e., with its detection probability close to the upper bound, and the pGLRT approaches the iGLRT as DNR increases. The sGLRT detector is outperformed by the former two detectors. In the case of $\mathrm{SNR} = 5$ dB, except for the mMF detector, all the remaining detectors perform well throughout the DNR region under test, with their detection probabilities close to 1. The mMF detector performs poorly at low DNR. This is again due to a mismatch: the PEV estimate assumes the presence of a strong DPI.

Fig. 3(d) shows the waveform estimation performance versus DNR in the same scenario as in Fig. 3(b). We can see that all the methods benefit from increasing DNR. From this figure, it is observed that the direct-path signal is not always an "interference" to a passive multistatic detection system. Since the DPI is a transformed replica of the IO waveform, utilizing it, instead of canceling it, can improve performance.

In Fig. 4(a), the detection performance is presented as a function of the channel number K, where $M = 20$, $\rho = 0.5$, $\mathrm{SNR} = 0$ dB, and $\mathrm{DNR} = 0$ dB. All detectors are seen to benefit from increasing K. In this scenario, the pGLRT detector approaches the iGLRT detector as the channel number increases, and both are very close to the clairvoyant MF. Without utilizing the waveform correlation, the sGLRT detector is outperformed by the proposed pGLRT detector. Fig. 4(b) shows the waveform estimation performance in the same setup. Obviously, the estimation performance of all methods improves as the channel number increases.

Fig. 5(a) illustrates the detection performance comparison versus the sample length M, where $K = 3$, $\rho = 0.5$, $\mathrm{SNR} = -5$ dB, and $\mathrm{DNR} = 0$ dB. We can see that increasing M leads to improved detection performance for all detectors. The performance of the pGLRT detector is very similar to that of iGLRT, which is close to the clairvoyant MF performance. The sGLRT detector is much worse without exploiting the waveform correlation. In Fig. 5(b), we also observe that all methods benefit from increasing the sample length, i.e., wider observation windows.

5.2. FM waveform

Besides the stochastic waveform with the Gaussian-shaped PSD, we also employ a practical FM signal as the IO waveform to test the performance of our detectors. The message signal is an audio signal which is frequency modulated by using a built-in Matlab function "fmmod". Since the exact covariance matrix of the FM waveform is unknown, the iGLRT detector is not included for comparison in this scenario. The detection performance versus SNR is shown in Fig. 6 where $M = 50$, $K = 3$, and $\mathrm{DNR} = 0$ dB. We see that the performance of the proposed pGLRT detector is close to the upper bound provided by the clairvoyant MF. The sGLRT detector performs about 2 dB worse than the pGLRT detector but is slightly better than the mMF in the low SNR region. Again, the performance degradation of the mMF detector is observed at high SNR, due to the poor waveform estimate of the PEV method. The mED and mGCC detectors have similar performance, which is about 6 dB worse than the pGLRT detector.

Fig. 7 shows the detection performance versus the sample length with $K = 3$, $\mathrm{SNR} = -5$ dB, and $\mathrm{DNR} = 0$ dB. Among all practical detectors, the pGLRT detector is still the one that is closest to the clairvoyant MF detector. The sGLRT detector is much worse without exploiting the correlation, especially when the sample length is small. The mMF performs slightly worse than the sGLRT but significantly better than the mED and mGCC. From these results, it is seen that the AR modeling is able to effectively capture and exploit the correlation of the FM waveform for passive detection.

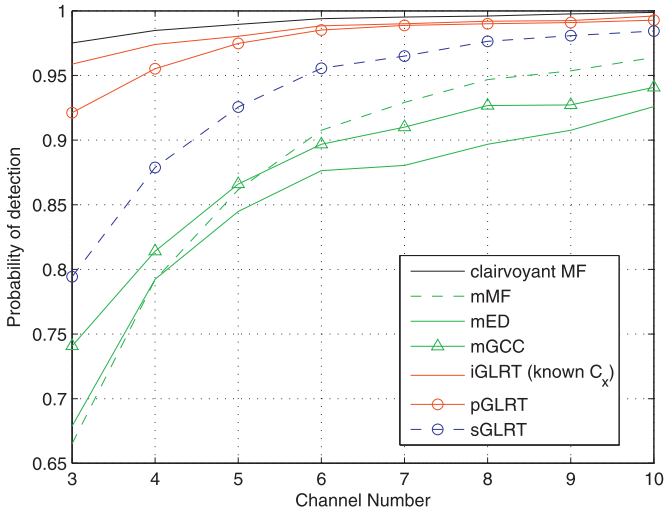

(a)

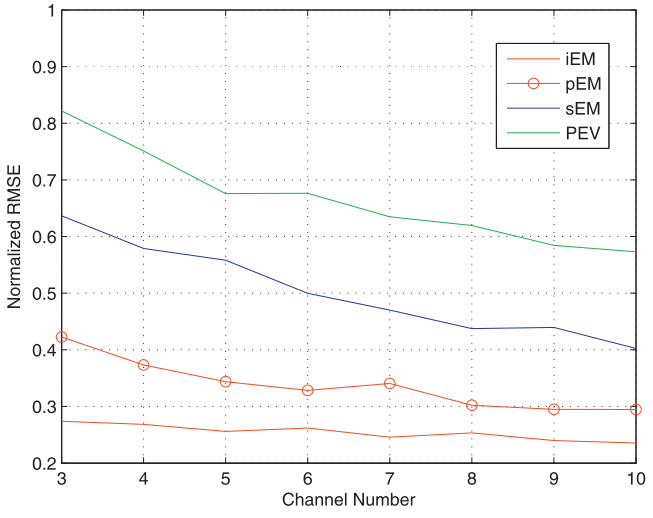

(b)

Fig. 4. Detection and estimation performance versus channel number K with $M = 20$, $\rho = 0.5$, SNR $= 0$ dB, and DNR $= 0$ dB. (a) Detection probability. (b) Normalized RMSE of waveform estimate.

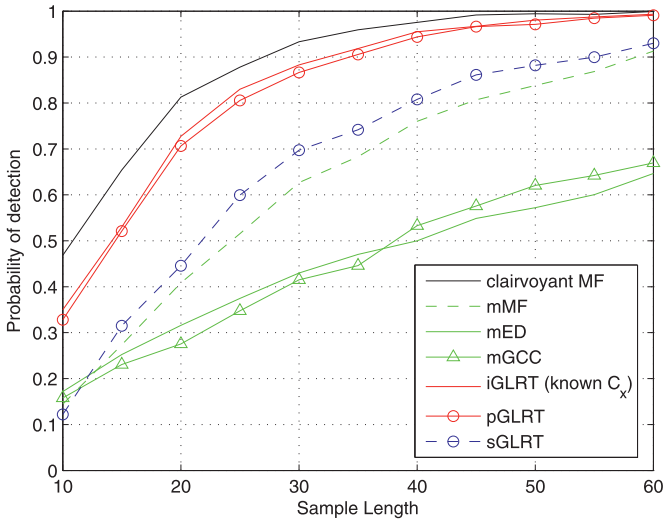

(a)

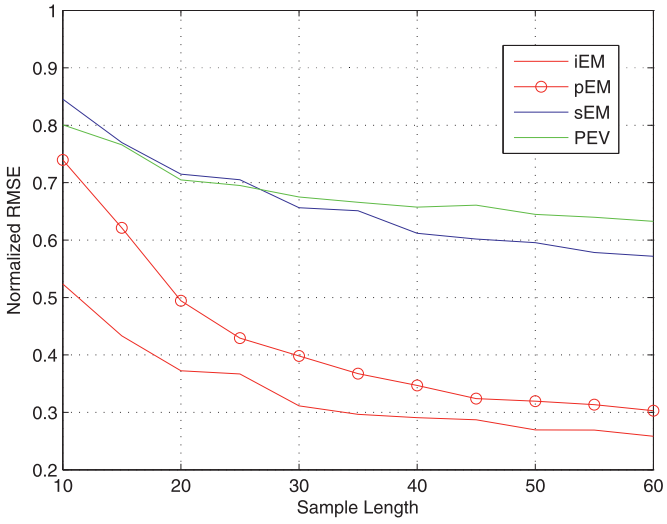

(b)

Fig. 5. Detection and estimation performance versus sample length M with $K = 3$, $\rho = 0.5$, SNR $= -5$ dB, and DNR $= 0$ dB. (a) Detection probability. (b) Normalized RMSE of waveform estimate.

6. Conclusion

In this paper, we considered the target detection problem for a multistatic passive radar system by exploiting the correlation of the IO waveform. We proposed a parametric GLRT approach, which models the waveform as an AR process, and the AR model is integrated in an EM framework for model order selection, parameter estimation, and detection. We also derived a clairvoyant MF detector, which provides a performance upper bound, and several modified detectors based on the clairvoyant MF and conventional solutions by accounting for DPI in the observations. These detectors have been extensively tested using both stochastic waveforms with a Gaussian-shaped PSD and FM waveforms as the IO signals. Numerical results show that the performance of the proposed parametric GLRT is very close to that of the clairvoyant MF detector and significantly outperforms the other detectors which ignore the IO waveform correlation.

Appendix A. Proof of (15)–(18)

Under $\mathcal{H}_1$, we have the unknown parameters $\boldsymbol{\theta} = \{\boldsymbol{\alpha}, \boldsymbol{\beta}, \boldsymbol{\eta}, \mathbf{a}, \sigma^2\}$, and the likelihood function of the "complete" data $\mathbf{z} = [\mathbf{x}^T, \mathbf{y}^T]^T$ can be written as

$$p(\mathbf{z}|\boldsymbol{\theta}) = p(\mathbf{y}|\mathbf{x}, \boldsymbol{\theta}) p(\mathbf{x}|\boldsymbol{\theta}) \approx \frac{1}{(\pi\sigma^2)^{M-P} \det\{\pi \mathbf{C}_n(\boldsymbol{\eta})\}} \times \exp\left\{ -\frac{\|\mathbf{x}_P + \mathbf{X}_P \mathbf{a}\|^2}{\sigma^2} - \sum_{k=1}^{K} \frac{\|\mathbf{y}_k - \beta_k \mathbf{x} - \alpha_k \mathcal{D}_k \mathbf{x}\|^2}{\eta_k} \right\}, \quad (53)$$

where

$$\mathbf{x}_m = [x(m+1), x(m+2), \ldots, x(m+M-P)]^T, \quad (54)$$

for $m = 0, 1, \ldots, P$, and

$$\mathbf{X}_P = [\mathbf{x}_{P-1}, \mathbf{x}_{P-2}, \ldots, \mathbf{x}_0]. \quad (55)$$

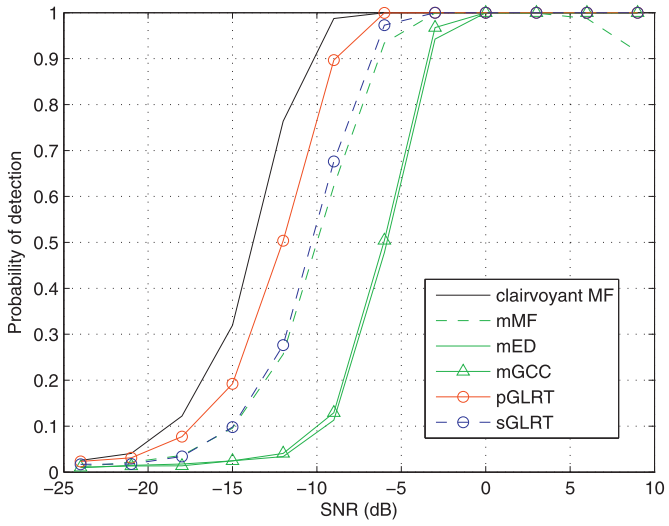

Fig. 6. Detection performance versus SNR using the FM waveform with $M = 50$, $K = 3$, and DNR = 0 dB.

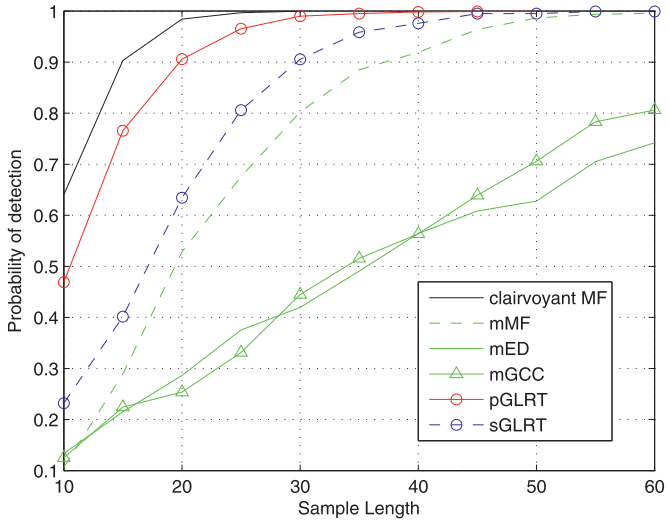

Fig. 7. Detection performance versus sample length M using the FM waveform with $K = 3$, SNR = −5 dB, and DNR = 0 dB.

Herein, we use the asymptotic form for the likelihood function of the waveform $p(\mathbf{x}|\boldsymbol{\theta})$, instead of the exact likelihood function, to avoid some cumbersome mathematical operations [32]. The LLF is thus given by

$$\log p(\mathbf{z}|\boldsymbol{\theta}) = s_1 - s_2(\mathbf{x}, \boldsymbol{\theta}), \tag{56}$$

where

$$s_1 = \quad [P - M(K+1)] \ln \pi, \tag{57}$$

$$s_2(\mathbf{x}, \boldsymbol{\theta}) = (M-P)\ln\sigma^2 + \frac{\Delta_1(\mathbf{x}, \mathbf{a})}{\sigma^2} + \sum_{k=1}^{K}\left(M \ln \eta_k + \frac{\Delta_2(\mathbf{x}, \alpha_k, \beta_k)}{\eta_k}\right), \tag{58}$$

with

$$\Delta_1(\mathbf{x}, \mathbf{a}) = \|\mathbf{x}_P + \mathbf{X}_P\mathbf{a}\|^2 = \mathbf{x}_P^H\mathbf{x}_P + \mathbf{x}_P^H\mathbf{X}_P\mathbf{a} + \mathbf{a}^H\mathbf{X}_P^H\mathbf{x}_P + \mathbf{a}^H\mathbf{X}_P^H\mathbf{X}_P\mathbf{a}, \tag{59}$$

$$\Delta_2(\mathbf{x}, \alpha_k, \beta_k) = \|\mathbf{y}_k\|^2 + \left(|\beta_k|^2 + |\alpha_k|^2\right)\mathbf{x}^H\mathbf{x} + 2\Re\left\{\alpha_k\beta_k^*\mathbf{x}^H\mathcal{D}_k\mathbf{x} - \beta_k\mathbf{y}_k^H\mathbf{x} - \alpha_k\mathbf{y}_k^H\mathcal{D}_k\mathbf{x}\right\}. \tag{60}$$

The cost function is consequently given by

$$Q\left(\boldsymbol{\theta}; \hat{\boldsymbol{\theta}}^{(l)}\right) = s_1 - E_{\mathbf{x}|\mathbf{y},\hat{\boldsymbol{\theta}}^{(l)}}\left\{s_2(\mathbf{x}, \boldsymbol{\theta})\right\}. \tag{61}$$

Note that only the second term in (61) involves the parameters to be estimated, and thus we have the following result for the M-step,

$$\arg\max_{\boldsymbol{\theta}} Q\left(\boldsymbol{\theta}; \hat{\boldsymbol{\theta}}^{(l)}\right) = \arg\min_{\boldsymbol{\theta}} Q_1\left(\boldsymbol{\theta}; \hat{\boldsymbol{\theta}}^{(l)}\right), \tag{62}$$

where

$$Q_1\left(\boldsymbol{\theta}; \hat{\boldsymbol{\theta}}^{(l)}\right) = E_{\mathbf{x}|\mathbf{y},\hat{\boldsymbol{\theta}}^{(l)}}\left\{s_2(\mathbf{x}, \boldsymbol{\theta})\right\}. \tag{63}$$

Next, we find an explicit expression for $Q_1\left(\boldsymbol{\theta}; \hat{\boldsymbol{\theta}}^{(l)}\right)$. Since the vectors $\mathbf{x}$ and $\mathbf{y}$ are jointly Gaussian distributed with zero mean, the posterior mean $\hat{\mathbf{x}}^{(l)} = E_{\mathbf{x}|\mathbf{y},\hat{\boldsymbol{\theta}}^{(l)}}\{\mathbf{x}\}$ has a closed-form expression [42, p. 324]. By denoting the partitioned covariance matrix of $\mathbf{z}$ as

$$\mathbf{C}_z^{(l)} = \begin{bmatrix} \mathbf{C}_{xx}^{(l)} & \mathbf{C}_{xy}^{(l)} \\ \mathbf{C}_{yx}^{(l)} & \mathbf{C}_{yy}^{(l)} \end{bmatrix}, \tag{64}$$

where

$$\mathbf{C}_{xx}^{(l)} = E\left\{\mathbf{x}\mathbf{x}^H; \hat{\boldsymbol{\theta}}^{(l)}\right\} = \mathbf{C}_x(\hat{\mathbf{a}}^{(l)}, \hat{\sigma^2}^{(l)}), \tag{65}$$

$$\mathbf{C}_{xy}^{(l)} = \left(\mathbf{C}_{yx}^{(l)}\right)^H = E\left\{\mathbf{x}\mathbf{y}^H; \hat{\boldsymbol{\theta}}^{(l)}\right\} = \left(\hat{\boldsymbol{\beta}}^{(l)}\right)^H \otimes \mathbf{C}_{xx}^{(l)} + \mathbf{C}_{xx}^{(l)}\left(\hat{\boldsymbol{\alpha}}^{(l)} \otimes \mathbf{I}_M\right)^H\mathbf{D}^H, \tag{66}$$

$$\mathbf{C}_{yy}^{(l)} = E\left\{\mathbf{y}\mathbf{y}^H; \hat{\boldsymbol{\theta}}^{(l)}\right\} = \mathbf{C}_y\left(\hat{\boldsymbol{\theta}}^{(l)}\right). \tag{67}$$

As mentioned before, the covariance matrix $\mathbf{C}_x(\hat{\mathbf{a}}^{(l)}, \hat{\sigma^2}^{(l)})$ is formed from the ACF sequence with its first element normalized, while the ACF function is computed by the Levinson–Durbin Algorithm (LDA) and the step-down (SD) procedure. Consequently, we have the posterior mean as

$$\hat{\mathbf{x}}^{(l)} = E\{\mathbf{x}\} + \mathbf{C}_{xy}^{(l)}\left(\mathbf{C}_{yy}^{(l)}\right)^{-1}(\mathbf{y} - E\{\mathbf{y}\}) = \mathbf{C}_{xy}^{(l)}\left(\mathbf{C}_{yy}^{(l)}\right)^{-1}\mathbf{y}, \tag{68}$$

and the posterior correlation matrix as

$$\mathbf{R}_{xx|y}^{(l)} = E_{\mathbf{x}|\mathbf{y},\hat{\boldsymbol{\theta}}^{(l)}}\left\{\mathbf{x}\mathbf{x}^H\right\} = \hat{\mathbf{x}}^{(l)}\left(\hat{\mathbf{x}}^{(l)}\right)^H + E_{\mathbf{x}|\mathbf{y},\hat{\boldsymbol{\theta}}^{(l)}}\left\{\left(\mathbf{x} - \hat{\mathbf{x}}^{(l)}\right)\left(\mathbf{x} - \hat{\mathbf{x}}^{(l)}\right)^H\right\} = \hat{\mathbf{x}}^{(l)}\left(\hat{\mathbf{x}}^{(l)}\right)^H + \mathbf{C}_{xx}^{(l)} - \mathbf{C}_{xy}^{(l)}\left(\mathbf{C}_{yy}^{(l)}\right)^{-1}\left(\mathbf{C}_{xy}^{(l)}\right)^H. \tag{69}$$

Denote

$$c_1^{(l)} = E_{\mathbf{x}|\mathbf{y},\hat{\boldsymbol{\theta}}^{(l)}}\left\{\mathbf{x}^H\mathbf{x}\right\} = \mathrm{tr}\left\{\mathbf{R}_{xx|y}^{(l)}\right\}, \tag{70}$$

$$c_{2,k}^{(l)} = E_{\mathbf{x}|\mathbf{y},\hat{\boldsymbol{\theta}}^{(l)}}\left\{\mathbf{x}^H\mathcal{D}_k\mathbf{x}\right\} = \mathrm{tr}\left\{\mathcal{D}_k\mathbf{R}_{xx|y}^{(l)}\right\}, \tag{71}$$

$$c_{3,k}^{(l)} = E_{\mathbf{x}|\mathbf{y},\hat{\boldsymbol{\theta}}^{(l)}}\left\{\mathbf{y}_k^H\mathbf{x}\right\} = \mathbf{y}_k^H\hat{\mathbf{x}}^{(l)}, \tag{72}$$

$$c_{4,k}^{(l)} = E_{\mathbf{x}|\mathbf{y},\hat{\boldsymbol{\theta}}^{(l)}}\left\{\mathbf{y}_k^H\mathcal{D}_k\mathbf{x}\right\} = \mathbf{y}_k^H\mathcal{D}_k\hat{\mathbf{x}}^{(l)}, \tag{73}$$

$$c_5^{(l)} = E_{\mathbf{x}|\mathbf{y},\hat{\boldsymbol{\theta}}^{(l)}}\left\{\mathbf{x}_P^H\mathbf{x}_P\right\} = \textstyle\sum_{i=P+1}^{M}\left[\mathbf{R}_{xx|y}^{(l)}\right]_{i,i}, \tag{74}$$

$$\mathbf{c}_6^{(l)} = E_{\mathbf{x}|\mathbf{y},\hat{\boldsymbol{\theta}}^{(l)}}\left\{\mathbf{X}_P^H\mathbf{x}_P\right\}, \tag{75}$$

where

$$\left[\mathbf{c}_6^{(l)}\right]_p = E_{\mathbf{x}|\mathbf{y},\hat{\boldsymbol{\theta}}^{(l)}}\left\{\mathbf{x}_{P-p}^H\mathbf{x}_P\right\} = \sum_{i=P+1}^{M}\left[\mathbf{R}_{xx|y}^{(l)}\right]_{i,i-p},\quad p=1,2,\ldots,P, \tag{76}$$

and

$$\mathbf{C}_7^{(l)} = E_{\mathbf{x}|\mathbf{y},\hat{\boldsymbol{\theta}}^{(l)}}\left\{\mathbf{X}_P^H\mathbf{X}_P\right\}, \tag{77}$$

where

$$\left[\mathbf{C}_7^{(l)}\right]_{p,q} = E_{\mathbf{x}|\mathbf{y},\hat{\boldsymbol{\theta}}^{(l)}}\left\{\mathbf{x}_{P-p}^H\mathbf{x}_{P-q}\right\} = \sum_{i=P+1}^{M}\left[\mathbf{R}_{xx|y}^{(l)}\right]_{i-q,i-p},\quad p,q=1,2,\ldots,P. \tag{78}$$

Finally, we get the expressions shown in (16)–(18).

Appendix B. Auto-correlation method

For easy reference, the auto-correlation method for AR coefficient estimation is summarized here. The AC method employs the following cost function[2] [35]

$$\Delta_3(\mathbf{x},\mathbf{a}) = \|\mathbf{x}_0+\mathbf{X}_P\mathbf{a}\|^2 = \mathbf{x}_0^H\mathbf{x}_0+\mathbf{x}_0^H\mathbf{X}_P\mathbf{a} + \mathbf{a}^H\mathbf{X}_P^H\mathbf{x}_0+\mathbf{a}^H\mathbf{X}_P^H\mathbf{X}_P\mathbf{a}, \tag{79}$$

where $\mathbf{X}_P=[\mathbf{x}_1,\mathbf{x}_2,\ldots,\mathbf{x}_P]$ and $\mathbf{x}_m=[\mathbf{0}_{1\times m},\mathbf{x}^T,\mathbf{0}_{1\times(P-m)}]^T$, $m=0,1,\ldots,P$. As a result, we have

$$\mathbf{c}_6^{(l)} = E_{\mathbf{x}|\mathbf{y},\hat{\boldsymbol{\theta}}^{(l)}}\left\{\mathbf{X}_P^H\mathbf{x}_0\right\}, \tag{80}$$

where

$$\left[\mathbf{c}_6^{(l)}\right]_p = E_{\mathbf{x}|\mathbf{y},\hat{\boldsymbol{\theta}}^{(l)}}\left\{\mathbf{x}_p^H\mathbf{x}_0\right\} = \sum_{i=p+1}^{M}\left[\mathbf{R}_{xx|y}^{(l)}\right]_{i,i-p},\quad p=1,2,\ldots,P, \tag{81}$$

and

$$\mathbf{C}_7^{(l)} = E_{\mathbf{x}|\mathbf{y},\hat{\boldsymbol{\theta}}^{(l)}}\left\{\mathbf{X}_P^H\mathbf{X}_P\right\}, \tag{82}$$

where

$$\left[\mathbf{C}_7^{(l)}\right]_{p,q} = E_{\mathbf{x}|\mathbf{y},\hat{\boldsymbol{\theta}}^{(l)}}\left\{\mathbf{x}_p^H\mathbf{x}_q\right\} = \begin{cases}\sum_{i=q-p+1}^{M}\left[\mathbf{R}_{xx|y}^{(l)}\right]_{i-q+p,i}, & q\geq p\\ \sum_{i=p-q+1}^{M}\left[\mathbf{R}_{xx|y}^{(l)}\right]_{i,i-p+q}, & p>q\end{cases}, \quad p,q=1,2,\ldots,P. \tag{83}$$

The $(l+1)$th update of the AR coefficients is then computed by equation (19).

References

[1] H.D. Griffiths, C.J. Baker, Passive coherent location radar systems. part 1: performance prediction, IEE Proc. Radar Sonar Navig. 152 (3) (2005) 124–132.
[2] P.E. Howland, D. Maksimiuk, G. Reitsma, FM radio based bistatic radar, IEE Proc. Radar Sonar Navig. 152 (3) (2005) 107–115.
[3] L. Wang, B. Yazici, Passive imaging of moving targets using sparse distributed apertures, SIAM J. Imaging Sci. 5 (3) (2012) 769–808.
[4] S. Gogineni, M. Rangaswamy, B.D. Rigling, A. Nehorai, Ambiguity function analysis for UMTS-based passive multistatic radar, IEEE Trans. Signal Process. 62 (11) (2014) 2945–2957.
[5] T. Shan, S. Liu, Y.D. Zhang, M.G. Amin, R. Tao, Y. Feng, Efficient architecture and hardware implementation of coherent integration processor for digital video broadcast-based passive bistatic radar, IET Radar Sonar Navig. 10 (1) (2016) 97–106.

[2] For brevity and some notational abuse, we use similar symbols as in Appendix A which are defined slightly differently.

[6] Q. He, R.S. Blum, The significant gains from optimally processed multiple signals of opportunity and multiple receive stations in passive radar, IEEE Signal Process. Lett. 21 (2) (2014) 180–184.
[7] Q. He, J. Hu, R.S. Blum, Y. Wu, Generalized Cramér-Rao bound for joint estimation of target position and velocity for active and passive radar networks, IEEE Trans. Signal Process. 64 (8) (2016) 2078–2089.
[8] H.-Y. Zhao, J. Liu, Z.-J. Zhang, H. Liu, S. Zhou, Linear fusion for target detection in passive multistatic radar, Signal Process. (Elsevier) 130 (2017) 175–182.
[9] J. Liu, H. Li, B. Himed, On the performance of the cross-correlation detector for passive radar applications, Signal Process. (Elsevier) 113 (2015) 32–37.
[10] D.E. Hack, L.K. Patton, B. Himed, M.A. Saville, Detection in passive MIMO radar networks, IEEE Trans. Signal Process. 62 (11) (2014) 2999–3012.
[11] G. Cui, J. Liu, H. Li, B. Himed, Signal detection with noisy reference for passive sensing, Signal Process. (Elsevier) 108 (2015) 389–399.
[12] D.E. Hack, C.W. Rossler, L.K. Patton, Multichannel detection of an unknown rank-N signal using uncalibrated receivers, IEEE Signal Process. Lett. 21 (8) (2014a) 998–1002.
[13] D.E. Hack, L.K. Patton, B. Himed, M.A. Saville, Centralized passive MIMO radar detection without direct-path reference signals, IEEE Trans. Signal Process. 62 (11) (2014b) 3013–3023.
[14] J. Liu, H. Li, B. Himed, Two target detection algorithms for passive multistatic radar, IEEE Trans. Signal Process. 62 (22) (2014) 5930–5939.
[15] P. Setlur, S. Gogineni, M. Rangaswamy, Waveform extraction from reference channels of passive multistatic radar systems, in: Proceedings of 49th Asilomar Conference on Signals, Systems and Computers, Pacific Grove, CA, 2015.
[16] I. Santamaria, L.L. Scharf, D. Cochran, J. Via, Passive detection of rank-one signals with a multiantenna reference channel, in: Proceedings of 2016 24th European Signal Processing Conference (EUSIPCO), Budapest, Hungary, 2016. Aug. 29–Sept. 2
[17] Y. Wang, L.L. Scharf, I. Santamaria, H. Wang, Canonical correlations for target detection in a passive radar network, in: Proceedings of 50th Asilomar Conference on Signals, Systems and Computers, Pacific Grove, CA, USA, 2016.
[18] X. Zhang, H. Li, J. Liu, B. Himed, Joint delay and Doppler estimation for passive sensing with direct-path interference, IEEE Trans. Signal Process. 64 (3) (2016) 630–640.
[19] O. Rabaste, D. Poullin, Rejection of Doppler shifted multipaths in airborne passive radar, in: Proceedings of 2015 IEEE International Radar Conference, Arlington, VA, USA, 2015, pp. 1660–1665.
[20] D.K.P. Tan, M. Lesturgie, H. Sun, Y. Lu, Target detection performance analysis for airborne passive bistatic radar, in: IEEE International Geoscience and Remote Sensing Symposium, 2010, pp. 3553–3556.
[21] F. Colone, D.W. O'Hagan, P. Lombardo, C.J. Baker, A multistage processing algorithm for disturbance removal and target detection in passive bistatic radar, IEEE Trans. Aerosp. Electron.Syst. 45 (2) (2009) 698–722.
[22] J.E. Palmer, H.A. Harms, S.J. Searle, L.M. Davis, DVB-T passive radar signal processing, IEEE Trans. Signal Process. 61 (8) (2013) 2116–2126.
[23] S. Searle, J. Palmer, L. Davis, D.W. O'Hagan, M. Ummenhofer, Evaluation of the ambiguity function for passive radar with OFDM transmissions, in: Proceedings of the 2014 IEEE Radar Conference, Cincinnati, OH, 2014, pp. 1040–1045.
[24] Y. Ma, T. Shan, Y.D. Zhang, M.G. Amin, R. Tao, Y. Feng, A novel two-dimensional sparse-weight NLMS filtering scheme for passive bistatic radar, IEEE Geosci. Remote Sens. Lett. 13 (5) (2016) 676–680.
[25] R. Tao, H.Z. Wu, T. Shan, Direct-path suppression by spatial filtering in digital television terrestrial broadcasting-based passive radar, IET Radar Sonar Navig. 4 (6) (2010) 791–805.
[26] A.P. Dempster, N.M. Laird, D.B. Rubin, Maximum likelihood from incomplete data via the EM algorithm, J. R. Stat. Soc. Ser. B (Methodological) 39 (1) (1977) 1–38.
[27] X. Zhang, H. Li, B. Himed, Multistatic detection for passive radar with direct–path interference, IEEE Trans. Aerosp. Electron.Syst. 53 (2) (2017) 915–925.
[28] M.A. Berezina, D. Rudoy, P.J. Wolfe, Autoregressive modeling of voiced speech, in: IEEE International Conference on Acoustics, Speech and Signal Processing, Dallas, TX, 2010.
[29] K.E. Baddour, N.C. Beaulieu, Autoregressive modeling for fading channel simulation, IEEE Trans. Wireless Commun. 4 (4) (2005) 1650–1662.
[30] J.R. Román, M. Rangaswamy, D.W. Davis, Q. Zhang, B. Himed, J.H. Michels, Parametric adaptive matched filter for airborne radar applications, IEEE Trans. Aerosp. Electron.Syst. 36 (2) (2000) 677–692.
[31] P. Wang, H. Li, B. Himed, A simplified parametric GLRT for STAP detection, in: Proceedings of the 2009 IEEE Radar Conference, Pasadena, CA, 2009, pp. 1–5.
[32] S.M. Kay, Modern Spectral Estimation: Theory and Application, Englewood Cliffs, NJ: Prentice Hall, 1988.
[33] K.S. Bialkowski, I.V.L. Clarkson, S.D. Howard, Generalized canonical correlation for passive multistatic radar detection, in: Proceedings of the 2011 IEEE Statistical Signal Processing Workshop (SSP), 2011, pp. 417–420.
[34] M.A. Richards, Fundamentals of Radar Signal Processing, McGraw-Hill, 2005.
[35] P. Stoica, R.L. Moses, Spectral Analysis of Signals, Upper Saddle River, NJ: Pearson Prentice Hall, 2005.
[36] T. Söderström, P. Stoica, System Identification, London, UK: Prentice Hall International, 1989.
[37] P. Wang, J. Fang, N. Han, H. Li, Multiantenna-assisted spectrum sensing for cognitive radio, IEEE Trans. Veh. Technol. 59 (4) (2010) 1791–1800.
[38] N. Vankayalapati, S. Kay, Asymptotically optimal detection of low probability of intercept signals using distributed sensors, IEEE Trans. Aerosp. Electron.Syst. 48 (1) (2012) 737–748.

[39] D. Cochran, H. Gish, D. Sinno, A geometric approach to multiple-channel signal detection, IEEE Trans. Signal Process. 43 (9) (1995) 2049–2057.
[40] Q. He, N.H. Lehmann, R.S. Blum, A.M. Haimovich, MIMO radar moving target detection in homogeneous clutter, IEEE Trans. Aerosp. Electron.Syst. 46 (3) (2010) 1290–1301.
[41] M.I. Skolnik, Introduction to Radar Systems, 3rd ed. New York, NY: McGraw-Hill, 2001.
[42] S.M. Kay, Fundamentals of Statistical Signal Processing: Estimation Theory, Upper Saddle River, NJ: Prentice Hall, 1993.